

Jeans Instability in a Tidally Disrupted Halo Satellite Galaxy

Justin Comparetta & Alice C. Quillen

Department of Physics and Astronomy, University of Rochester, Rochester, NY 14627, USA; jcompare@pas.rochester.edu

11 October 2021

ABSTRACT

We use a hybrid test particle/N-body simulation to integrate 4 million massless test particle trajectories within a fully self-consistent 10^5 particle N-body simulation. The number of massless particles allows us to resolve fine structure in the spatial distribution and phase space of a dwarf galaxy as it is disrupted in the tidal field of a Milky Way type galaxy. The tidal tails exhibit nearly periodic clumping or a smoke-like appearance. By running simulations with different satellite particle mass, halo particle mass, number of massive and massless particles and with and without a galaxy disk, we have determined that the instabilities are not due to numerical noise, amplification of structure in the halo, or shocking as the satellite passes through the disk of the Galaxy. We measure Jeans wavelengths and growth timescales in the tidal tail and show that the Jeans instability is a viable explanation for the clumps. We find that the instability causes velocity perturbations of order 10 km/s. Clumps in tidal tails present in the Milky Way could be seen in stellar radial velocity surveys as well as number counts. We find that the unstable wavelength growth is sensitive to the simulated mass of dark matter halo particles. A simulation with a smoother halo exhibits colder and thinner tidal tails with more closely spaced clumps than a simulation with more massive dark matter halo particles. Heating by the halo particles increases the Jeans wavelength in the tidal tail affecting substructure development, suggesting an intricate connection between tidal tails and dark matter halo substructure.

1 INTRODUCTION

There is evidence for past and ongoing accretion of small objects by the Milky Way halo, the most dramatic object being the disrupted Sagittarius dwarf galaxy (Ibata et al. 1994). Disrupting satellites leave behind tidal tails and, on longer timescales, stellar streams (Bekki & Freeman 2003; Helmi et al. 2003; Meza et al. 2005; Penarrubia et al. 2005; Purcell et al. 2007; Helmi 2008). Previous studies of stellar streams have used N-body simulations to study the disruption and evolution of merging galaxies (e.g., Helmi et al. 2006; Johnston et al. 2008; Gomez & Helmi 2010). However, most previous simulations have not placed many particles in the disrupting object itself. A large number of particles is required to resolve structure in the velocity distribution in a small local volume (e.g., Minchev et al. 2009; Gomez & Helmi 2010). After satellite disruption, satellite particles are distributed all over the Galaxy.

Early simulations of dwarf galaxy disruption necessarily contained few particles. The focus of many of these simulations was constraining the orientation and shape of the halo from observations of the Sagittarius Dwarf stream rather than searching for substructure in the tails themselves. The simulations by Johnston et al. (1996); Johnston (1998) contained only 10^4 particles in the dwarf galaxy and those by

Helmi et al. (2006) only had 5000 particles. The simulations by Bullock & Johnston (2005) had 10^4 massive particles but an additional 1.2×10^5 massless test particles in their dwarf satellites. The simulations discussed by Gomez & Helmi (2010) are described in more detail by Villalobos & Helmi (2008) and contained 3×10^5 particles in the satellite.

While substructure in the form of clumps has not been detected in the Sag Dwarf streams, it has been seen in tidal tails associated with smaller objects. Clumped structure observed in the tidal debris of the globular cluster Palomar 5 (Odenkirchen et al. 2002) is interpreted in terms of oscillations in the cluster (Gnedin et al. 1999) caused by a previous passage through the Galactic disk (Odenkirchen et al. 2002; Dehnen et al. 2004), epicyclic perturbations excited during tidal disruption (Kupper et al. 2008) and Jeans instability (Quillen & Comparetta 2010). Alternative possibilities accounting for structure in cluster tidal tails include the effect of dark matter subhalos, as explored by Ibata et al. (2002); Mayer et al. (2002); Johnston et al. (2002); Penarrubia et al. (2006); Siegal-Gaskins & Valluri (2008); Carlberg (2009).

Here, we strive to carry out N-body simulations with a larger number of particles placed in the disrupting dwarf galaxy. We use the simulations to look in detail at the structure of the tidal tails during and following disruption from the dwarf galaxy.

2 NUMERICAL INTEGRATIONS

We first describe the N-body integrator used. We then describe our modifications to the integrator that allow us to simultaneously integrate test (massless) particles. We then describe the initial conditions used in our simulations and list the different simulations carried out.

2.1 Hybrid N-body and test particle integration

The N-body integrator used is a direct-summation code called ϕ GRAPE (Harfst et al. 2007) that employs a 4th order Hermite integration scheme with hierarchical commensurate block timesteps (Makino & Aarseth 1992). Instead of using special purpose GRAPE hardware, we use the the Sapporo subroutine library (Gaburov et al. 2009) that closely matches the GRAPE-6 subroutine library (Makino et al. 2003) but allows the force and jerk computations to be done on graphics processing units (GPUs). Force computation is done in double precision, though jerk computation is not.

We have modified the integrator so that massless particles can be integrated simultaneously along with the massive particles. This is done by adding an extra parameter to the ϕ GRAPE code, $N_{massive}$, that is the number of massive particles. The massless and massive particles are integrated together but only the massive particles are part of the j data set used to calculate the forces and jerks (Makino et al. 2003). The GRAPE-6 subroutine library passes n_j massive particles to the GRAPE boards (or in our case to the GPU) with the subroutine call *g6_set.j.particle* (see the GRAPE-6 User guide¹). Instead of passing all particles, we pass the total number of massive particles, $N_{massive}$, to this routine. The accelerations and jerks on the i particles are computed by summing terms from each of the n_j particles; this is done in the GRAPE-6 subroutines *g6calc_firsthalf* and *g6calc_lasthalf* that are called in the gravity computation step of ϕ GRAPE. The number of j particles in these two subroutine calls is also changed to $N_{massive}$. The remaining computation steps, e.g., the predictor step, the corrector step and the identification of active particles, remain unchanged and are done on all particles.

Computation of accelerations and jerks in an N-body simulation require $O(N^2)$ computations for N particles. In our hybrid code $O(N_{massive}^2)$ computations are done on the massive particles and $O(N_{massive} \times N_{massless})$ are done on the massless particles. For example a simulation of 10^5 massive and 10^7 massless particles would require $O(10^{12})$ computation steps. This is less than integrating 10^7 massive particles, which would require $O(10^{14})$ computation steps. Thus, the hybrid scheme is a way to integrate additional particles and better resolve structure in phase space while not compromising the speed of the simulation. The hybrid scheme adopted here made it possible for us to integrate 4 million dwarf galaxy particles during tidal disruption in the context of a self-consistent N-body simulation with a live halo on a desktop computer containing off the shelf graphics cards. While test particle simulations can simulate this number of trajectories without difficulty (e.g., Minchev et

al. 2009; Quillen et al. 2009), test particle simulations alone (not combined with N-body) are not self-consistent.

The test-particle/N-body hybrid scheme used here is similar to the particle cloning technique often used in celestial mechanics integrations to improve understanding of statistical properties of orbits (e.g., Kaib et al. 2009; Masaki & Kinoshita 2003). Test particles have been used previously to better resolve structure in cosmological simulations. For example, those by Bullock & Johnston (2005) placed 1.2×10^5 test particles in their dwarf galaxies which contained only 10^4 massive particles.

2.2 Initial conditions

Initial particle distributions were created separately for the Milky Way type galaxy and the dwarf galaxy.

The initial conditions for the model Milky Way were made with a numerical phase distribution function using the method discussed by Widrow et al. (2008) and their numerical routines which are described by Kuijken & Dubinski (1995); Widrow & Dubinski (2005); Widrow et al. (2008). The code computes a gravitational potential for bulge, disk and halo components, then computes a distribution function for each component. N-body initial condition files are then computed for each component. The galactic bulge is consistent with a Sersic law for the projected density. The halo profile has cusp strength γ . The disk falls off exponentially with radius and as a sech^2 with height. Parameters are those for the standard Milky Way model, listed in Table 2 by Widrow et al. (2008).

The number of massive particles in each of the bulge, disk, halo and dwarf components are shown in Table 1. The total mass of the disk is $5.31 \times 10^{10} M_\odot$, the bulge is $8.27 \times 10^9 M_\odot$, and the halo is $4.42 \times 10^{11} M_\odot$. The halo is live.

The dwarf galaxy initial conditions were created using a King model. The model is described by 2 parameters, a velocity dispersion, σ^2 , and a concentration, c . The concentration, $c = r_t/r_0$, is the ratio of the tidal radius, r_t , setting the outer boundary to the core radius, r_0 . Of interest is the central density $\rho_0 = \frac{9\sigma^2}{4\pi Gr_0^2}$. This central density sets the approximate location of complete tidal disruption in the background galaxy. In Table 2 we list the properties of the dwarf galaxy. The total mass of the dwarf galaxy is $2.70 \times 10^8 M_\odot$.

The initial conditions of each simulations are identical except for the following changes. Run 1 has a lower number of massive particles present in the dwarf galaxy than the other 3 runs, though the total mass in the dwarf is the same. Run 2 is our standard run. Run 3 and 4 have 10 times more dark matter particles than the Runs 1 and 2, though the total halo mass is the same in all runs. Run 4 is lacking a disk. There is a small but insignificant change in the number of massless particles in the dwarf galaxy in Run 3.

2.3 Orbit

We choose a polar orbit for the dwarf satellite. The initial position of the satellite is 15 kpc from the center of the Milky Way type galaxy along the direction of the plane of the disk, and 20 kpc perpendicular to the disc. The velocity is 200 km/s directed toward the disk. The orbital time is approximately 1 Gyr. The orbit of the dwarf can be seen

¹ <http://www.artcompsci.org/makino/software/GRAPE6/>

Table 1. Numbers of Particles in each Galactic Component

Simulation No.	Disk	Bulge	Halo	Dwarf _{massive}	Dwarf _{massless}
Run 1	77000	37000	8000	9072	4×10^6
Run 2	77000	37000	8000	60000	4×10^6
Run 3	77000	37000	80000	60000	3.94×10^6
Run 4	0	37000	80000	60000	4×10^6

Particle numbers for the four simulations. Total mass in the bulge, disk and halo components is the same for all runs (except for Run 4 which does not include a disk). When there are more particles in a given component the mass of each particle is lower. All particles in a given component have the same mass.

Table 2. King Satellite Model

Parameter	Value
c	0.672
r_0	0.5 kpc
ρ_0	$0.4M_\odot/\text{pc}^3$
σ	25 km/s

Parameters for the satellite are described by a King model with parameters above.

in the snapshots as shown in Figures 1, 2, & 3. Each figure corresponds to a separate run, with Figure 1 corresponding to Run 2, Figure 2 corresponding to Run 3, and Figure 3 corresponding to Run 4. The parameters of the King model for the satellite were adjusted so that the satellite produced strong tidal tails but did not completely disrupt during its first pericenter passage.

2.4 Additional details about the simulations

The softening length for all particles in all simulations was 0.1 kpc and was chosen to be the average initial spacing between dwarf galaxy particles. Total energy was conserved between 99.996% and 99.999% in all simulations. If the chosen softening length were larger we would have failed to see structure on kpc scales. If the softening length were chosen to be smaller we would have seen unrealistic acceleration of a small fraction of the particles to high velocities from close approaches.

All simulations were performed for a timescale of 3 Gyr on a single desktop computer with two GTX 295 GPUs. Each run took between 5 and 10 days.

3 RESULTS

We first discuss the morphology of the tidal tails as seen in the different runs. We compare tidal tail structure as a function of number of simulated massive particles in the dwarf and number of particles in the halo. We explore the possibility that the Jeans instability is the cause of the clumping apparent in the simulations.

3.1 Morphology

Snapshots from simulation Runs 2, 3, & 4 are shown in Figures 1, 2, & 3 respectively. Run 1 is not shown as it is visibly indistinguishable from Run 2. The figures show projections into the $x - z$ plane of number density (histograms)

in Galactocentric coordinates. The galaxy disk lies in the $z = 0$ plane or horizontally on these plots. All dwarf galaxy particles are included and both massive and test particles are shown. Halo, disk and bulge particles are not shown. Evolution of the dwarf galaxy is shown from 0.33 Gyr to the end of the simulation at 3.0 Gyr in increments of one-third Gyr. We saw no differences between massive and massless dwarf galaxy particle distributions so they are not displayed separately.

In these snapshots, it is evident that the tidally disrupted tails of the dwarf galaxy exhibit clumps, or nearly periodically spaced density enhancements. When viewed sequentially as a movie this effect appears almost smoke-like in behavior. The density enhancements can be seen in most of the snapshots past 1.0 Gyr, and more clearly in the left panels of Figures 6 and 7. The spacing between clumps is 2-5 kpc in Run 2 but shorter in Run 3 and of order 1-2 kpc. The density enhancements are in the form of nearly periodically spaced ridges that are oriented perpendicular to the orbit.

From comparisons of Run 1 to Run 2 we can test the possibility that this substructure is caused by heating within the tail itself and by the massive dwarf galaxy particles in the tail. For Run 2 we use a factor of 6.6 times more massive particles in the dwarf galaxy than in Run 1 so the mass of each dwarf particle is 6.6 times larger in Run 1 than Run 2. Yet the two simulations have similar morphologies. Noise caused by low numbers of massive particles in the dwarf is not likely responsible for the clumping.

Run 2 and Run 3 are the same except that Run 3 contains more halo particles. The mass of each halo particle in Run 2 is $5.5 \times 10^7 M_\odot$ whereas each halo mass in Run 3 is a tenth of this. Here we do see a difference between the tidal tail morphologies. Run 3 (with lower mass halo particles) has denser and narrower tails. Previous simulations have seen thickening of tidal tails caused by heating from subhalos (Ibata et al. 2002; Mayer et al. 2002; Johnston et al. 2002; Penarrubia et al. 2006). The wider tails seen in Run 2 (Figure 1) compared to those Run 3 (Figure 2) are consistent with heating caused by the larger masses of the halo particles in Run 2. The mass of our halo particles in Run 2 is similar to the lowest mass subhalos simulated by Ibata et al. (2002). Their simulations were carried out in a smooth static background potential but included softened subhalos.

Previous simulations have found that dark matter subhalos can also cause structure in a tidal tail (Siegal-Gaskins & Valluri 2008; Carlberg 2009). Siegal-Gaskins & Valluri (2008) also used a smooth static background potential and included subhalos with masses in the range of $6 \times 10^6 -$

$6 \times 10^8 M_\odot$ as well as a smaller number of halo particles with masses up to 4.6×10^{10} . Clumps in the tails can be excited by nearby dark matter subhalos (see Figure 3 by Siegal-Gaskins & Valluri 2008). Here, however, we see more prominent but also more closely spaced clumps in tails when the dark matter particles are of lower mass (Run 3; see Figure 2). The larger number of clumps in Run 3 compared to Run 2 suggests that the dark matter particles are not the cause of the substructure. Siegal-Gaskins & Valluri (2008) saw clumps in the tails that were simulated in a smooth static potential and lacked subhalos (see their Figure 3 top left panel). This suggests that if we were to carry out simulations in a smooth potential (or with more and even lower mass halo particles) that we would continue to see clumps.

Run 4 lacks a stellar disk. In this simulation (see Figure 3) we still see clumping in the tails. However, as the clumping is still present in Run 4 we conclude that shocking from passage through the disk is not the cause. Note that the difference in the orbit shown in Figure 3 from Figures 1 & 2 is to be expected as the simulation is missing the potential from the galactic disk.

In summary, our simulations show periodic clumping in the tidal tails of a disrupting dwarf satellite. By comparing two simulations with different numbers of massive particles in the dwarf we rule out amplification of numerical noise from massive particles in the tails as an explanation for clumps. The simulation lacking a galactic disk also exhibits clumps, thus disk shocking cannot account for the tail structure. The mass of the dark matter particles does affect the tail morphology, but in a way opposite to that expected. When the halo particles are more massive the clumps are smaller and more closely spaced rather than larger, suggesting that heating by the halo has reduced the extent of the clumping instability.

We note that the clumps we see in the tidal tails would be difficult to see in a simulation containing fewer dwarf galaxy particles. Most previous simulations may have lacked the substructure we see here because they had fewer particles in the dwarf galaxy. It is possible that the simulations by Siegal-Gaskins & Valluri (2008) do display Jeans instabilities (see Figures 8 and 13 which may show periodic clumps) however it is not easy to tell as they plotted each particle individually rather than made histograms as we have done here.

3.2 Jeans Instability

Self gravity could be responsible for the substructure seen in the simulated tidal tails. To test this hypothesis we measure the Jeans wavelength at different regions in the tails and times during the simulations.

The Jeans wavelength is

$$\lambda_J \equiv \sqrt{\frac{\pi \sigma^2}{G \rho_0}}. \quad (1)$$

Planar perturbations on wavelengths longer than the Jeans wavelength are unstable and grow on a timescale

$$t_{growth} \sim (4\pi G \rho_0)^{-1/2} \quad (2)$$

whereas those wavelengths shorter than the Jeans wavelength are damped via a process similar to Landau damping (e.g. Chap. 5, Binney & Tremaine 1987).

If the Jeans instability is responsible for the clumping then prior to clump formation we should find that the Jeans wavelength is comparable to the distance between the clumps.

Formally, the growth timescale is infinite at the Jeans wavelength. However, perturbations at all wavelengths larger than the Jeans wavelength are unstable. The wavelength of maximum growth rate should be larger than but of order of the Jeans wavelength (e.g., Fridman & Polyachenko 1984; Binney & Tremaine 1987; Quillen & Comparetta 2010). The exact growth rate, however, is non-trivial to predict for the case where the wavenumber of the perturbation times the width of the tail is on order or greater than 1, as seen in Quillen & Comparetta (2010) for the regime investigated in these simulations. We expect that unstable perturbations with wavelength just longer than the Jeans wavelength are those with the fastest growth.

3.2.1 Measuring Jeans wavelength and growth rates

We calculate the Jeans wavelength using both massive and massless particles in the tidal tail. Including only the massive particles results in an insufficient particle sample to compute the velocity dispersion in a bin small enough to resolve the substructure. Since we include both massive and massless particles in computing the density ρ_0 in Equation 1, we normalize the density by the ratio of massless plus massive to massive particles. We include only those particles within a half kpc of the plane containing the dwarf galaxy orbit (the $y = 0$ plane). In bins of 0.25×0.25 kpc in the x, z directions and 1 kpc wide in the y direction we computed sums involving both the massive and massless particles. To estimate the density in the bin, we count the number of particles, multiply by the mass of the massive particles and divide by the ratio of the number of massless plus massive to massive particles. The velocity dispersion in the bin was computed from all particles in the bin and using all velocity components. The Jeans wavelength was then computed from the mass density and velocity dispersion using equation 1.

Growth rates are computed from the mass density using equation 2. The growth rate is calculated for the same regions that were used in computing the Jeans lengths. Here only the massive particles were included in the computation of the growth rate as we only require the density and we did not need to estimate the local velocity dispersion.

Jeans wavelengths computed in the tails at different timesteps are shown in Figure 4 and Figure 5. At the same timesteps and locations in the tail we also show the growth timescales and projected density.

In Figure 4 the top left panel shows the Jeans wavelength for the tidally disrupted dwarf in Run 2 at a timestep of 0.46 Gyr. For the upper right portion of the tail, there are sections of the tidal tail that have Jeans lengths of 2–3 kpc. This is similar to the spacing between the clumps seen later in the simulation and is shown in the projected density in Figure 4 in the bottom right panel.

In Figure 4 the top right panel shows the growth rate in Gyr for the same sections of the tidal tail used in the computation of the Jeans length in the top left panel. For the same sections of the tidal tail that had Jeans lengths of 2–3 kpc, the growth rate is about 0.2–0.3 Gyr.

If the observed clumping is due to the Jeans instability,

we should see clumping become evident in the simulation after about a growth timescale. The two bottom panels in Figure 4 show projected number densities of all particles in the tidally disrupted dwarf. The bottom left panel is a snapshot at the same time as the upper panels, at 0.46 Gyr, while the bottom right panel is at 0.82 Gyr. Clumping has formed within 0.36 Gyr as expected from the growth rate estimate, and the clumps are about 3.5–4 kpc apart as would be expected from the Jeans wavelengths exhibited by the tail earlier in the simulation.

The same progression is illustrated for Run 3 in Figure 5 for the simulation with lower mass halo particles. Here the upper right portion of the tail has a Jeans length of around 2 kpc in the upper left panel, and a growth time scale for that region of 0.3–0.4 Gyr is seen in the upper right panel. Although no clumping is seen in the projected density in the lower left panel at 0.47 Gyr, clumps have formed in the tail a growth timescale later. These are shown in the bottom right panel at 0.87 Gyr and have a shorter spacing (compared to Figure 4) as expected from the shorter Jeans wavelength exhibited earlier.

Within the context of first order linear perturbation theory (e.g., Binney & Tremaine 1987) the growth timescale for the Jeans instability is the inverse of an exponential growth rate. If perturbations present in the tail are small, then they would require many exponential growth timescales before they cause detectable density contrasts. However, we see substructure in a time that is only on the order of a single growth timescale. There are two factors that may be contributing to this. The original perturbations that grow may not be small, and examination of the density at early times in the simulation suggests that this may be the case. Gravitational collapse can be self-similar (Shu 1977). As the growth is expected to be non-linear the density contrast may become high on a single collapse timescale.

To summarize, we find that the spacings between the clumps are consistent with Jeans wavelengths measured earlier during the simulation. The delay timescale is similar to the growth timescales needed to develop the instability. This suggests that the Jeans instability is a viable explanation for the periodic substructure we see in our simulations.

3.3 Features in velocity space

The periodically spaced over-densities are visible in space coordinates and so could be visible in stellar number counts on the sky. However removal of background number counts introduces noise in a measurement of density in a tidal tail (e.g., Yanny et al. (2009)). As background number counts may be high it may be difficult to detect low amplitude density density perturbations in a tidal tail from number counts alone. Here we consider the possibility that the clumps also cause structure in the radial velocity field.

In Figures 6 & 7, for Run 2 and Run 3, respectively, we have plotted radial velocity versus radius (right panels, in galactocentric coordinates) for several sections of the tidal tails exhibiting clumping (shown in number density plots in the left panels). In these figures, we show on the left the projected density for small regions of the tidal tail. For each panel on the left there is a corresponding panel on the right showing the distribution of radial velocity v_r versus galactocentric radius r . The radial velocity component would be

consistent with a radial velocity measurement by an observer near the Galactic center. We chose these components to roughly illustrate phenomena that would be seen for a distant tidal stream as observed from the Sun. However we did not project components from a specific location outside the galactic center which would have required us to specify an arbitrary location within the context of this simulation.

In Figures 6 & 7, the same regions which display substructure (clumps) in spatial coordinates also exhibit substructure in the velocity plots. It is important to note that though we have plotted the velocity in the radial direction of a spherical galactocentric coordinate, we find that the velocity gradient points along the path of the orbit and is consistent with compression along the tidal tail and along the orbit. These plots should not be misinterpreted in terms of bending of the tail.

In Figures 6 & 7, the densest regions in the left hand panels show the density corresponds to bright vertical regions on the v_r vs r plots shown on the right. These regions have larger ranges in the radial velocity component, so larger velocity dispersions. The clumps have larger velocity dispersions than inter-clump regions.

Steps in the v_r vs r plots correspond to changes in the mean velocity. Steps are particularly visible in the bottom right hand panel of Figure 6. The smooth drop in velocity with increasing radius in the bottom right hand panel is caused by the orbit. If one was to subtract a smooth mean curve from this panel a sinusoidal-like oscillation would remain. This corresponds to positive and negative velocity perturbations about the mean orbital velocity. After subtraction the zeros of the sinusoidal oscillation lie in the inter-clump region. These correspond to velocities diverging from the mean orbital velocity. The maxima of the sinusoidal oscillation correspond to clumps where the velocities are converging. Thus, the motions are diverging in the interclump regions and converging in the clumps. This is the motion expected for longitudinal compressive motions oriented along the direction of the orbit and along the tail.

From the mass continuity equation, we can check whether the velocity in the tail is consistent with the growth timescales for clumping. The mass continuity equation is

$$\frac{\partial \rho}{\partial t} + \nabla \cdot (\rho \mathbf{v}) = 0. \quad (3)$$

To order of magnitude this gives, $\frac{\Delta \rho}{\Delta t} \approx \rho \frac{\Delta v}{\Delta x}$ where Δx is the spacing between clumps, $\Delta \rho$ the difference between clump and inter clump density, Δv the size of the velocity perturbations and Δt the timescale of the instability. Solving for Δv :

$$\Delta v \sim \frac{\Delta x \Delta \rho}{\Delta t \rho}. \quad (4)$$

For spacing between the clumps, Δx , of 3 kpc, growth timescales, Δt , of 0.3 Gyr, and a density contrast, $\Delta \rho / \rho$, of 2, we estimate a Δv of 20 km/s. This is about the size of the velocity jumps between the clumps in the panels shown in Figures 6 & 7, and implies that the velocity jumps we see in the simulation are consistent with compressive motions on the growth timescale of the instability.

We note that the clumps have larger velocity dispersion compared to the interclump velocity dispersions. This implies that the Jeans wavelength measured after the clumps have grown is larger than that present prior to the growth of

the instability. When we measure the Jeans wavelength in a region exhibiting clumps we find that it is much larger than the spacing between the clumps. This is not necessarily a contradiction as the current clumps grew when the tail was colder. Not surprisingly, the growth of the instability itself heats the tail as gravitational energy is converted to kinetic energy. However, this does present a problem for calculating a Jeans wavelength from an observed tail that already exhibits the instability in the form of clumping. When we calculate the Jeans wavelength from the regions shown after clump formation in Figures 4 & 5 we find that it exceeds the distance between the clumps. As there is an increase in the velocity dispersion caused by the instability, it is likely that tidal tails can be thickened by the growth of Jeans instabilities. This is possibly an issue in the interpretation of heating of tails from dark matter substructure alone (Ibata et al. 2002; Johnston et al. 2002; Siegal-Gaskins & Valluri 2008; Carlberg 2009).

Previous studies have found structure in phase space in tidal tails. For example, phase wrapping has caused clumps to appear in the velocity field (Helmi & deZeeuw 2000; Minchev et al. 2009). However, this process requires many orbital times to develop and appears in the velocity distribution after the tail has wrapped multiple times around the galaxy. Consequently this type of phase space structure is unlikely to be confused with the periodic features seen in the radial velocity plots shown in Figures 6 & 7.

In summary, we observe correlations between velocity dispersion, mean velocity and density in the tidal tails consistent with a compressive instability. Such correlations might in the future be used to identify clumping via the Jeans instability and heating from the Jeans instability to differentiate it from clumping due to halo substructure.

4 DISCUSSION

Here we discuss differentiating between the Jeans instability and other mechanisms of structure formation in tidal tails. We contrast our results with alternate explanations for clumping in tidal tails. Lastly, we compare our results with simulations shown in Siegal-Gaskins & Valluri (2008), which explore correlations between subhalos in the dark matter halo and substructure in tidal tails.

4.1 An alternate mechanism

An alternate explanation for the periodic over-densities in tidal tails was proposed by Kupper et al. (2008, 2010), where they attribute the cause of the clumping to epicyclic motions of the escaped stars in the tails. The clumps correspond to places where the stars in the tail slow down in their epicyclic motion.

The analytic models explored by Kupper et al. require the distance to the first over-density to be located some multiple of the tidal radius away from the core of the disrupting object. The time it takes the first clump to form is related to the inverse of the epicyclic frequency, and is the time it takes stripped stars to reach the distance to the first clump. After twice that duration, the stars have progressed twice as far and form a second over-density. Thus, in the case of a

circular orbit and constant tidal field (Kupper et al. 2008), after every multiple of this timescale another clump forms.

There are differences between the morphology we see in our simulations than that expected for epicyclic over-densities. Though the clumps in our simulations form at intervals similar to the tidal radius of the initial dwarf satellite, the distance to the first clump is much larger than the distance between the clumps. The periodic spacing between the clumps is not the same as the distance to the first clump as the epicyclic explanation would predict. Whereas the strength of the clumps decreases as a function of distance from the parent body, here we see strong clumps forming distant from the parent body. We find that the timing of the creation of the clumps in our simulations differ from that expected from an epicyclic explanation. Clumps in a region grow simultaneously, not in order of distance from the dwarf galaxy core. While epicyclic over-densities are a promising explanation for clumps seen in Palomar 5's tail they are unlikely to be the explanation for the clumps seen in the simulations presented here.

4.2 Halo substructure

Clumping in tidal debris has previously been investigated by Siegal-Gaskins & Valluri (2008), who found that subhalos were responsible for increased substructure in tidal tails. This can be seen in their sky projections in Figure 3 comparing star particles in simulations with and without the presence of subhalos. A smooth halo (top left panel of their Figure 3) produces less clumpy debris than a halo with substructure (top right panel). Similar to our simulations, they also find the substructure is observable in velocity space, as demonstrated in their Figure 6 showing radial velocity vs radius of their star particles, again in simulations with and without subhalos.

While most previous works (e.g., Ibata et al. (2002); Mayer et al. (2002); Johnston et al. (2002); Penarrubia et al. (2006); Carlberg (2009)) found that halo substructure heats tidal tails, Siegal-Gaskins & Valluri (2008) found in some cases that the tails in smooth halos were colder and denser than in halos with more substructure. It is possible that Jeans instability at shorter wavelengths was responsible for additional heating in these simulations. If so the connection between tidal tail and halo substructure may be more complex than previously considered.

5 SUMMARY AND CONCLUSION

We have used hybrid test particle/N-body integrations to increase the number of particles integrated within an N-body integrator so that we can more accurately resolve substructure. We have used our code to study the tidal disruption of a dwarf galaxy in a polar orbit of a Milky Way type galaxy. We have placed additional test particles in the dwarf galaxy so that we can resolve fine structure in the tidal tails.

In our simulations, we have found that stellar tidal tails can exhibit periodic ridges oriented perpendicular to the orbit. Such structure had not previously been noticed in similar N-body simulations, possibly because the tidal tails did not contain sufficient numbers of particles. However similar structure has been seen in simulations of tidal tails that

include gas (Wetzstein et al. 2007) and in this setting the clumps are interpreted in terms of a gravitational instability.

By comparing simulations with different numbers of massive dwarf and halo particles and with and without a disk, we have considered several explanations for the formation of clumps. We have ruled out the following methods for the formation of periodically spaced over-densities in our simulation: shocking by the galactic disk, numerical noise associated with under-populating the dwarf galaxy, amplification of structure in the halo, and epicyclic motions in the tidal tails.

We have measured the Jeans wavelength prior to the growth of the substructure and found that the tails are unstable to Jeans instability. The wavelengths of subsequently formed clumps are approximately consistent with the Jeans wavelength measured in the tail prior to formation. The timescale for growth is approximately consistent with the estimated growth timescale. These estimates suggest that Jeans instability is a viable interpretation of the clumps exhibited by our simulations. We find that the spacing between clumps is sensitive to the mass of our simulated dark matter halo particles. This is likely because heating by dark matter particles can increase the Jeans wavelength of the tidal tail.

We find that the clumps are also visible in a radial velocity projections suggesting that Jeans instabilities may be observable in tidal tails in our galaxy not only number counts but also in phase space using comparisons of radial velocity versus distance or position on the sky.

In the future, we expect increasingly rich data samples expanding the number of stars in the Milky Way with measured properties. These surveys may make it possible to probe for or rule out substructure in tidal tails such as exhibited by our simulations. If Jeans instabilities occur in tidal tails then associated heating caused by them should not be interpreted in terms of heating by halo substructure alone. Furthermore the fastest growing unstable wavelength may be sensitive to heating from the dark matter substructure implying that there may be a complex connection between halo and tidal tail substructure.

The simulations carried out here were made using a modest direct N-body code on a desktop computer. Future studies could test the results presented here with a more sophisticated N-body code (such as a tree code), and integrate more particles by doing the simulations on a supercomputer. Further studies can be carried out in different mass and stripping regimes for the disrupting object, such as globular clusters. We would also be interested in carrying out simulations that would more fully probe the possible connection between dark matter substructure and tidal tail morphology by simulating a more detailed halo than considered here.

We thank Larry Widrow for giving us and helping us with his code GalacticICS. We thank Jeff Bailin, Chris Purcell and Heidi Newberg for helpful communications. The King model was generated using code made available² by Sergey Mashchenko. We thank Evghenii Gaburov and Stefan Harfst for making ϕ GRAPE and Sapporo available. Support for this work was provided by NSF through award AST-0907841.

REFERENCES

- Bekki, K., & Freeman, K. C. 2003, MNRAS, 346, L11
 Binney, J. & Tremaine, S., 1987, "Galactic Dynamics," (Princeton:Princeton University Press)
 Bullock, J. S., & Johnston, K. V. 2005, ApJ, 635, 931
 Carlberg, R. G., ApJ, 705, 223
 Dehnen, W., Odenkirchen, M., Grebel, E. K., & Rix, H.-W. 2004, AJ, 127, 2753
 Fridman, A. M., & Polyachenko, V. L., 1984, "Physics of Gravitating Systems," Volume 1, (New York: Springer-Verlag)
 Gaburov, E., Harfst, S., & Portegies Zwart, S. 2009, New Astronomy, 14, 630
 Gnedin, O. Y., Lee, H. M., & Ostriker, J. P. 1999, ApJ, 522, 935
 frequencies
 Gomez, F. A., & Helmi, A. 2010, MNRAS, 401, 2285
 Harfst, S., Gualandris, A., Merritt, D., Spurzem, R., Portegies Zwart, S., & Berczik, P. 2007, New Astronomy, 12, 357.
 Helmi, A., & deZeeuw, P. T. 2000, MNRAS, 319, 657
 Helmi, A., Navarro, J. F., Meza, A., Steinmetz, M., & Eke, V. R. 2003, ApJ, 592, L25
 Helmi, A., Navarro, J. F., Nordstrom, B., Holmberg, J., Abadi, M. G., & Steinmetz, M. 2006, MNRAS, 365, 1309
 Helmi, A. 2008, A&ARv, 15, 145
 Ibata, R. A., Gilmore, G., & Irwin, M. J. 1994, Nature, 370, 194
 Ibata, R. A., Lewis, G. F., Irwin, M. J. & Quinn, T. 2002, MNRAS 332, 915
 Johnston, K. V., Hernquist, L., & Bolte, M. 1996, ApJ, 465, 278
 Johnston, K. V. 1998, ApJ, 495, 297
 Johnston, K. V., Spergel, D. N., & Haydn, C. 2002, ApJ, 570, 656
 Johnston, K. V., Bullock, J. S., Sharma, S., Font, A., Robertson, B. E., & Leitner, S. N. 2008, ApJ, 689, 936
 Kaib, N. A. et al. 2009, ApJ, 695, 268
 Kuijken, K., & Dubinski, J. 1995, MNRAS, 277, 1341
 Kupper, A. H. W., Macleod, A., & Heggie, D. C. 2008, MNRAS, 387, 1248
 Kupper, A. H. W., Kroupa, P., Baumgardt, H., & Heggie, D. C. 2010, MNRAS, 401, 105
 Makino, J., & Aarseth, S. J. 1992, PASJ, 44, 141
 Makino, J., Fukushige, T., Koga, M., & Namura, K. 2003, PASJ, 55, 1163
 Masaki, Y., & Kinoshita, H. 2003, A&A, 403, 769

² <http://www.physics.mcmaster.ca/~syam/software.html>

- Mayer, L., Moore, B., Quinn, T., Governato, F., & Stadel, J. 2002, MNRAS, 336, 119
- Meza, A., Navarro, J. F., Abadi, M. G., & Steinmetz, M. 2005, MNRAS, 359, 93
- Minchev, I., Quillen, A. C., Williams, M., Freeman, K. C., Nordhaus, J., Siebert, A., & Bienayme, O. 2009, MNRAS, 396, 56
- Odenkirchen, M., Grebel, E. K., Dehnen, W., Rix, H.-W., & Cudworth, K. M. 2002, AJ, 124, 1497
- Penarrubia, J., Martinez-Delgado, D., Rix, H. W., Gomez-Flechoso, M. A., Munn, J., Newberg, H., Bell, E. F., Yanny, B., Zucker, D., & Grebel, E. K. 2005, ApJ, 626, 128
- Penarrubia, J., Benson, A. J., Martinez-Delgado, D., Rix, H. W. 2006, ApJ, 645, 240
- Purcell, C. W., Bullock, J. S., & Zentner, A. R. 2007, ApJ, 666, 20
- Quillen, A. C., Minchev, I., Bland-Hawthorn, J., & Haywood, M. 2009, MNRAS, 397, 1599
- Quillen, A. C. & Comparetta, J. 2010, arXiv:1002.4870
- Shu, F. H. 1977, ApJ, 214, 488
- Siegal-Gaskins, J. M., & Valluri, M. 2008, ApJ, 681, 40
- Villalobos, A. & Helmi, A. 2008, MNRAS, 391, 1806
- Wetzstein, M., Naab, T., & Burkert, A. 2007, MNRAS, 375, 805
- Widrow, L. M., & Dubinski, J. 2005, ApJ, 631, 838
- Widrow, L. M., Pym, B., & Dubinski, J. 2008, ApJ, 679, 1239
- Yanny, B. et al. 2009, ApJ, 700, 1282

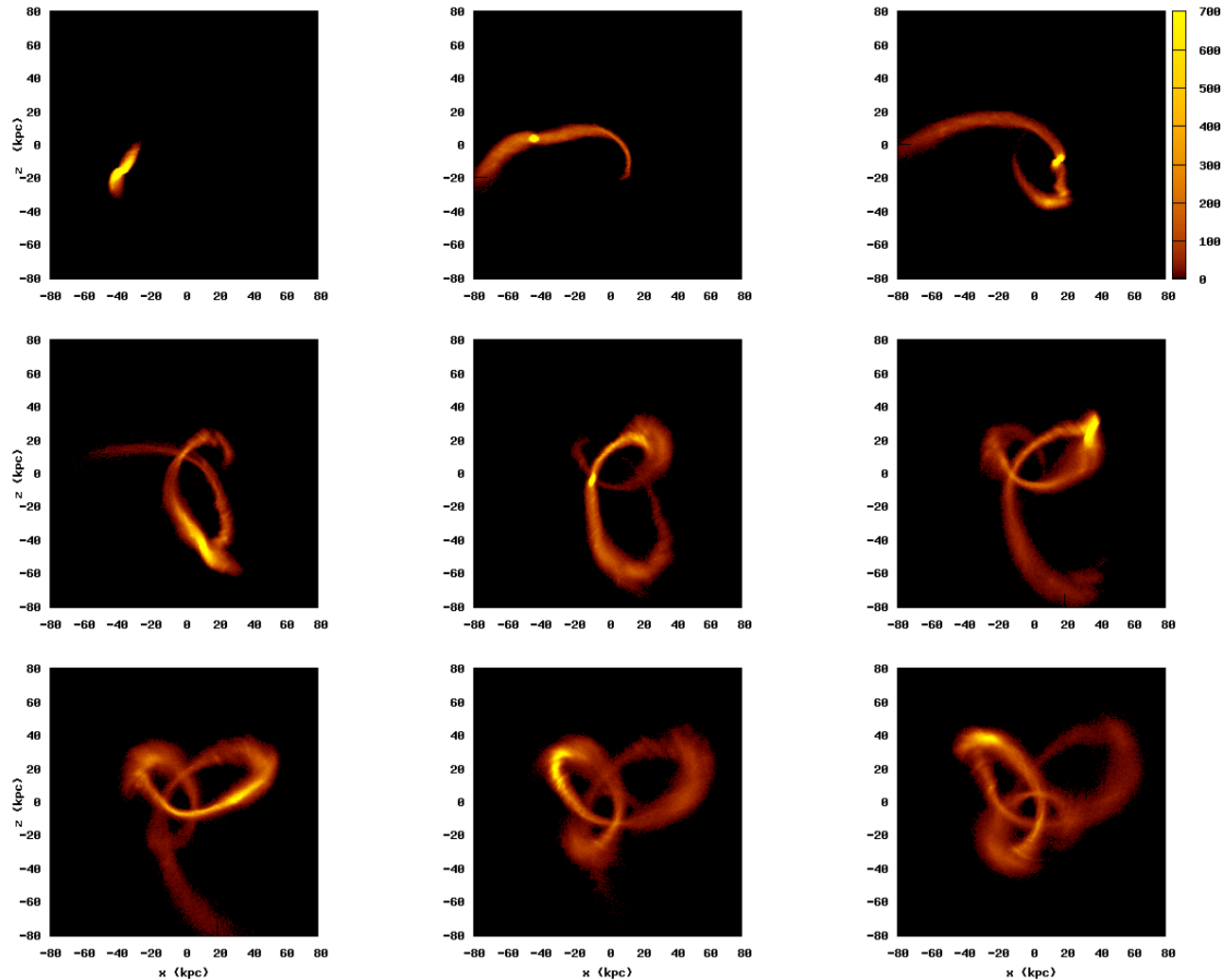


Figure 1. Snapshots showing projected number density of particles from the dwarf satellite in Run 2. Particles are shown projected onto the $x - z$ plane. The satellite is in a clockwise polar orbit with a Milky Way type galaxy centered at the origin containing a disk lying in the $z = 0$ plane (oriented horizontally in the figure). Disk, halo and bulge particles are not shown. The orbit is shown from 0.33 to 3 Gyr with a time of 0.33 Gyr between snapshots. Note the development of substructure in the tidal tail which can be seen in all panels past 1.0 Gyr, and most visibly at 2.66 Gyr (middle panel, bottom row). Substructure is in the form of nearly periodically spaced density enhancements. In the regions with periodic substructure, there is no change in tail width between clump and interclump regions; density variations are ridges perpendicular to the orbit caused by longitudinal or compressive motions along the direction of the orbit.

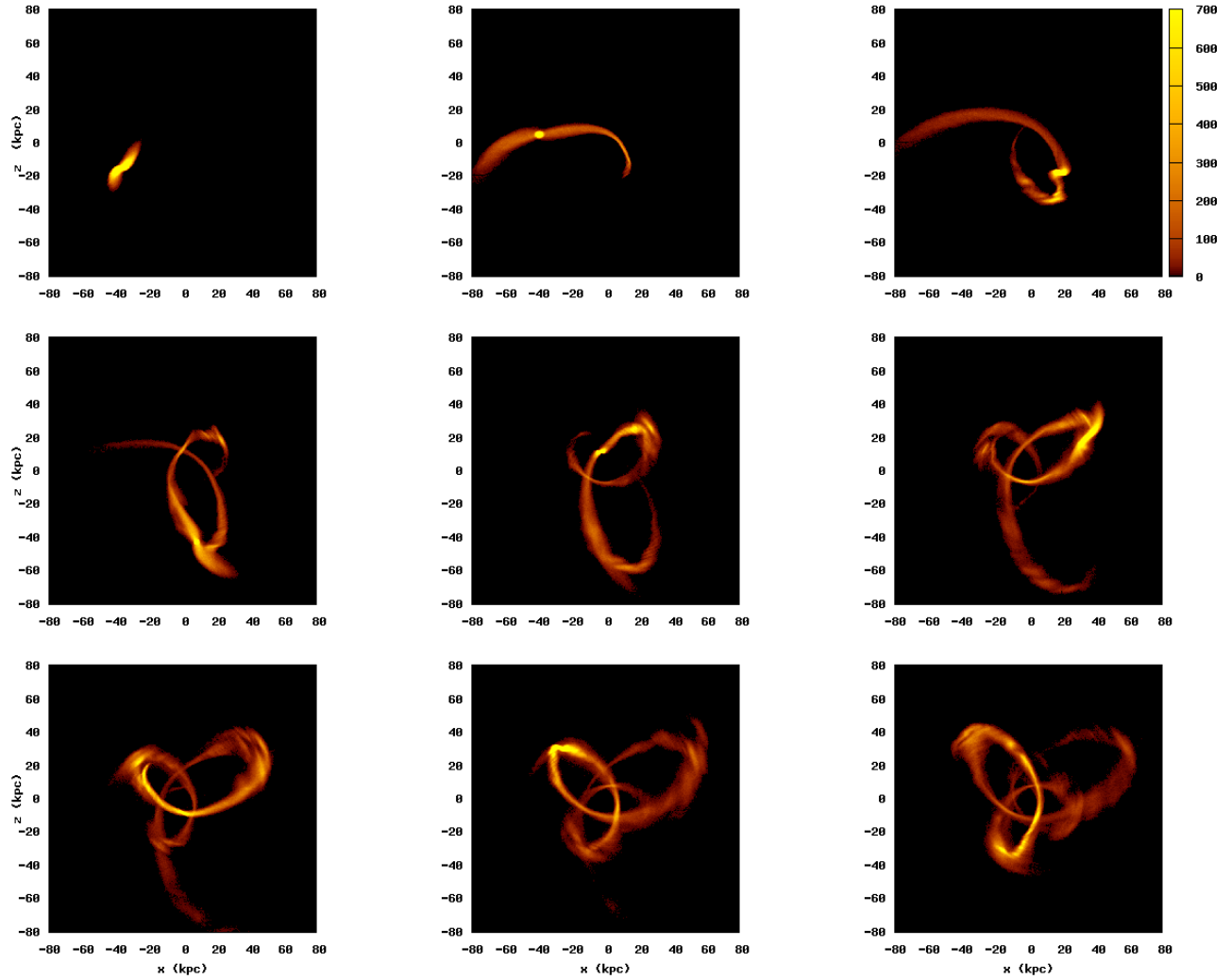


Figure 2. Snapshots showing projected number density of the dwarf satellite particles in Run 3. Similar to Figure 1. This simulation has 10 times as many dark matter halo particles as that shown in Figure 1; however, the orbit and mass distributions are identical. Tidal tails in this simulation are narrower and denser than in Run 2; this suggests that the halo particles have heated the tidal tails more in Run 2 than Run 3 due to their larger mass. The substructure in the tidal tails shown here is more prominent and displays more clearly defined and closely spaced ridges.

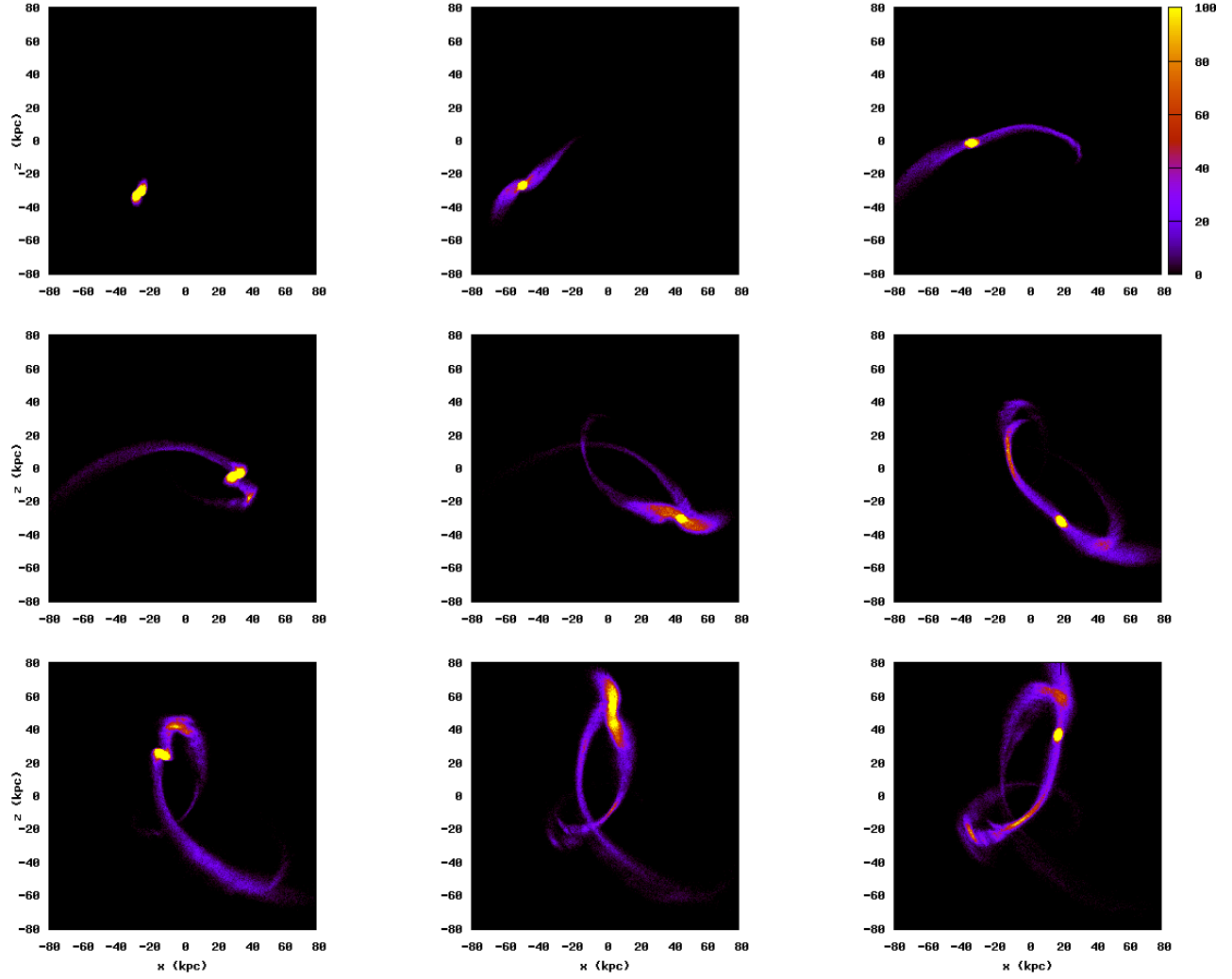


Figure 3. Snapshots showing projected number density of the dwarf satellite particles in Run 4. Similar to Figure 1. This simulation does not contain a galactic disk. However, substructure is seen in the tidal tails suggesting that disk shocking is not the cause for the density enhancements seen in Runs 1–3.

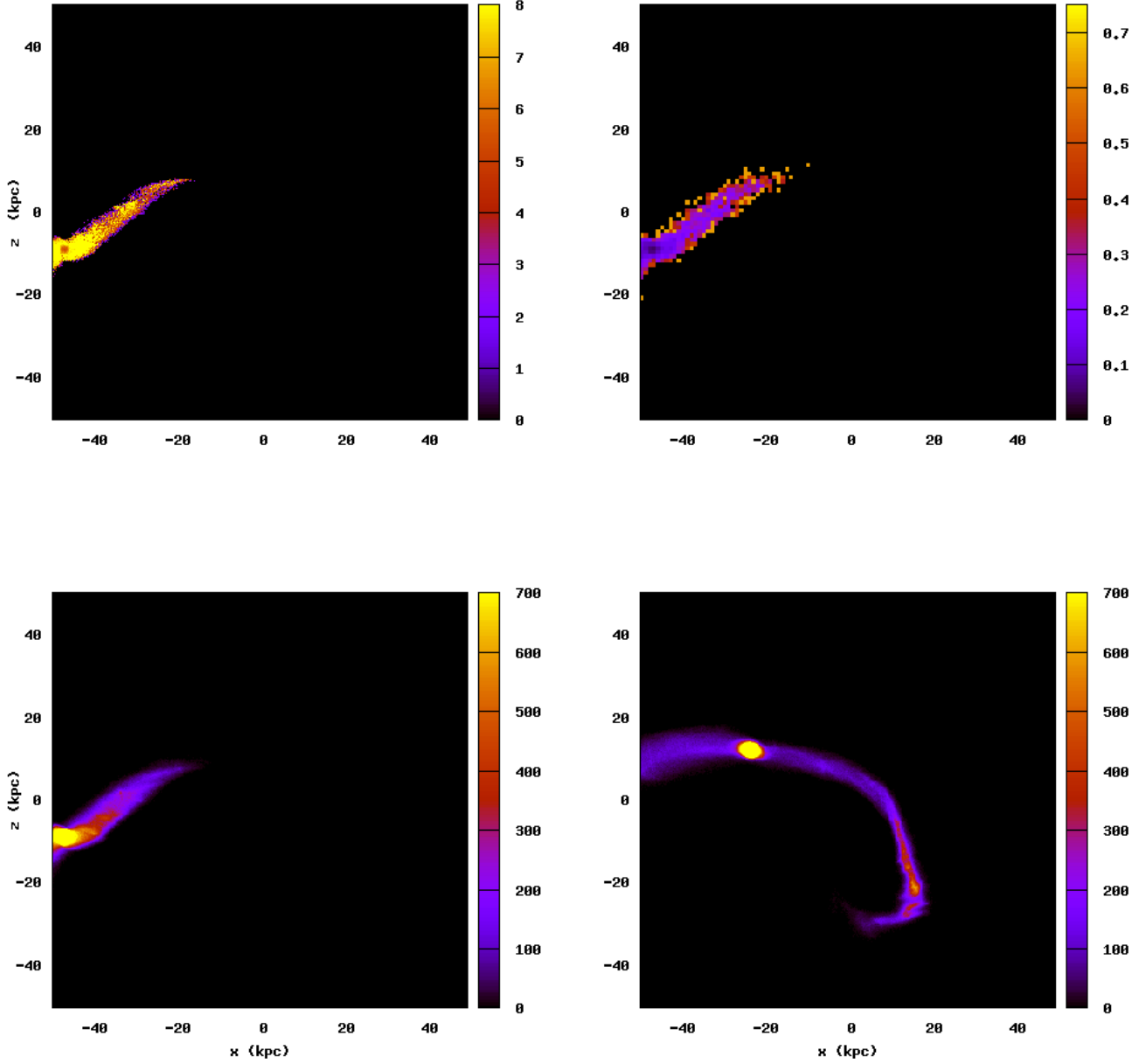


Figure 4. Top left panel: Jean's length of the tidal tail from Run 2 in kpc at the 0.46 Gyr timestep. The Jeans length is computed in each 0.25×0.25 kpc region in the xz plane for all particles within 0.5 kpc of the $y = 0$ plane containing the polar orbit of the satellite. We see regions which are Jeans unstable for wavelengths greater than 2–3 kpc. Top right panel: Growth timescale in Gyr for the same region, at the same time and in the same bins. Growth timescales for the instability are about 0.2–0.3 Gyr. Lower left panel: Number density of the tidal tail for the same time and region integrated along the y -direction. Lower right panel: Number density of tidal tail at 0.82 Gyr which is 0.36 Gyr after the snapshots shown in other three panels and about 1 instability growth timescale later. Substructure at the Jean's wavelength has grown in the tail in the expected timescale.

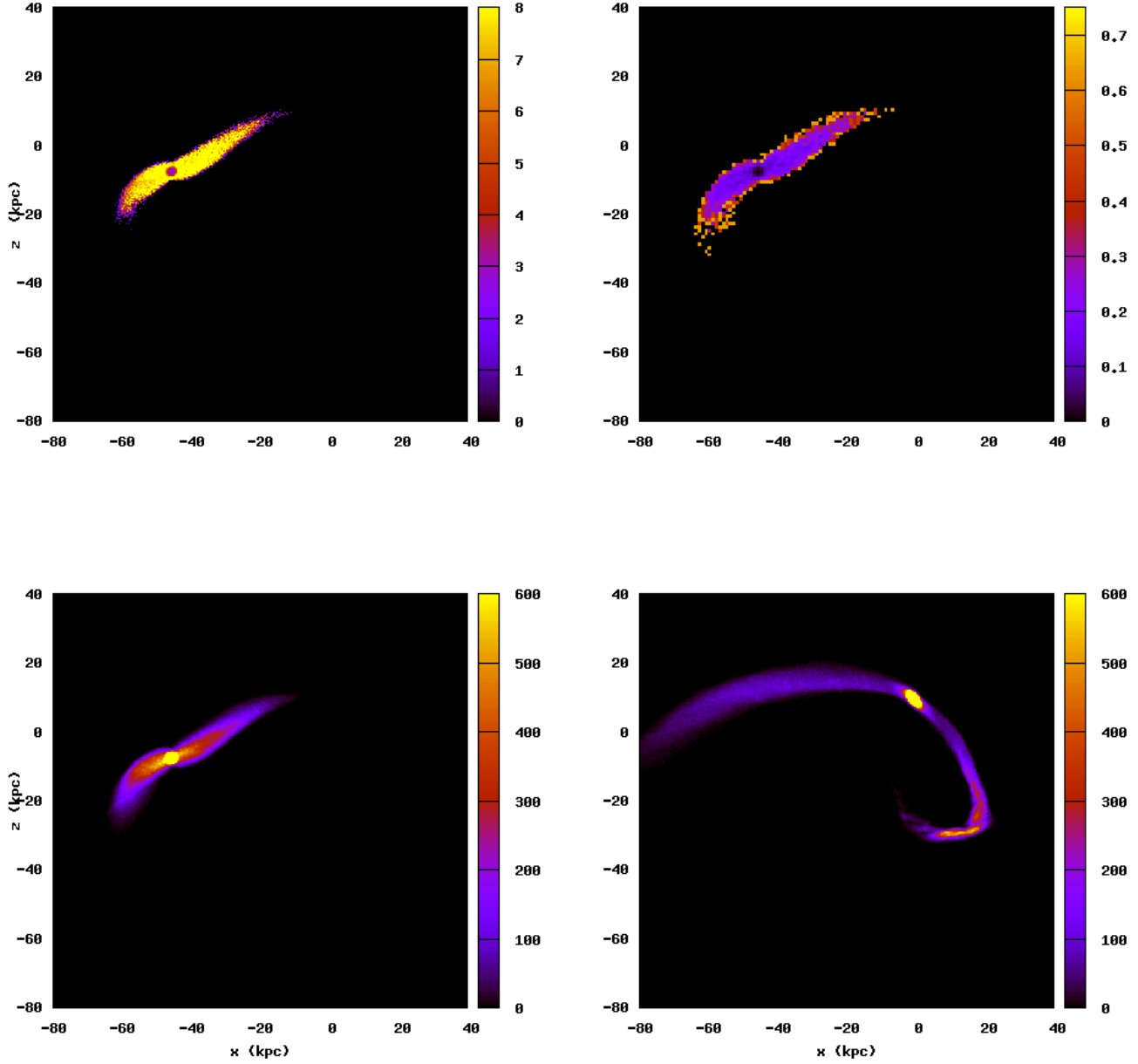


Figure 5. Top left panel: Jeans length of the tidal tail from Run 3 in kpc at 0.47 Gyr. This Figure is similar to Figure (4). We see regions which are Jeans unstable for wavelengths greater than 2 kpc. Top right panel: Growth timescale in Gyr for tidal tail for the same timestep. Growth timescales for this instability for the same region are about 0.3–0.4 Gyr. Lower left panel: Number density of tidal tail for the same timestep integrated along the y -direction. Lower right panel: Number density of tidal tail at 0.87 Gyr and 0.4 Gyr after the previous three panels. Structure at the Jean's wavelength has grown in the expected timescale.

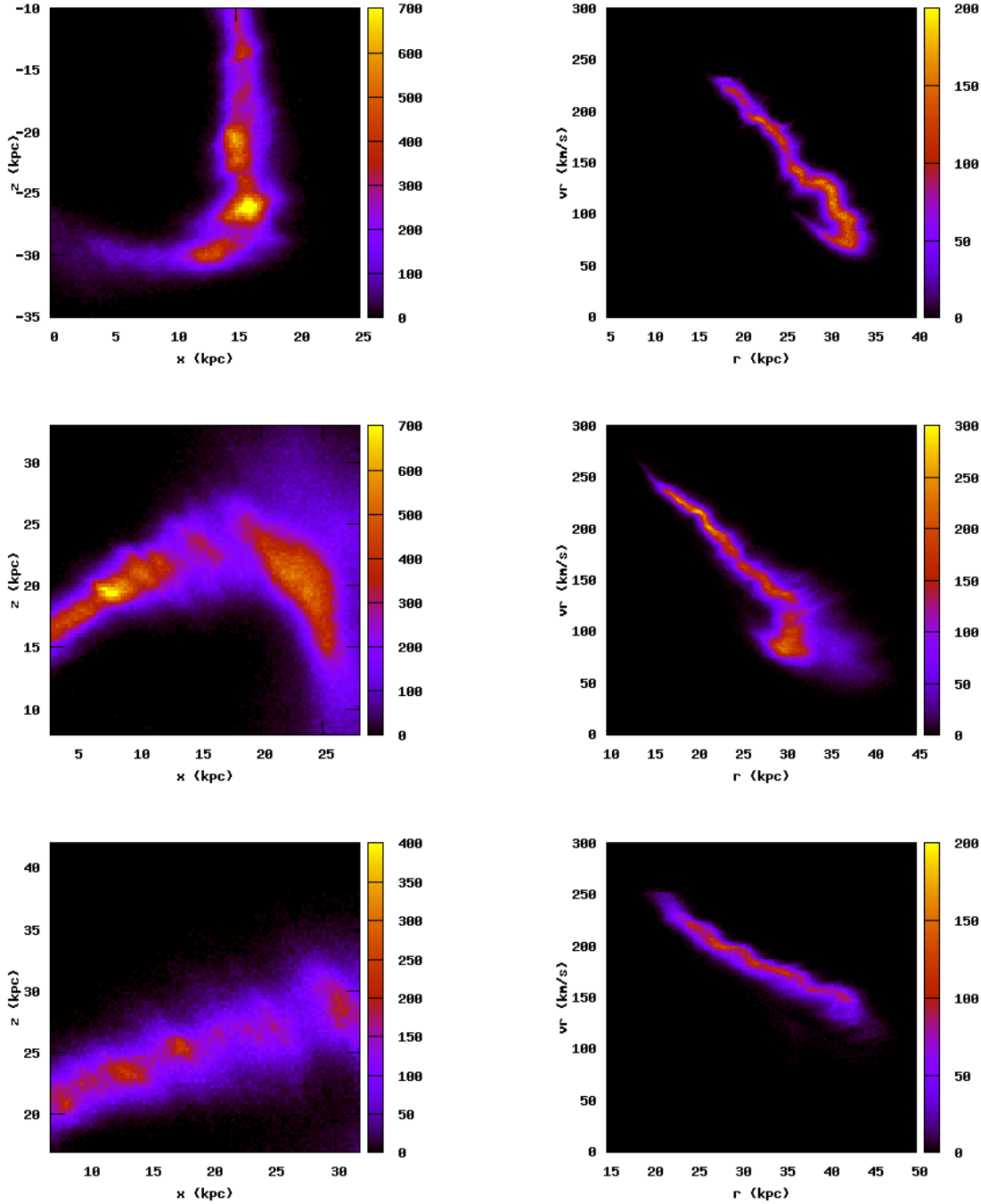


Figure 6. Left panels: Projected number densities at 3 different locations and times in Run 2 (0.86, 1.70, and 2.08 Gyr from top to bottom). We have chosen regions with prominent clumping in the tidal tails. Right panels: For particles shown on each left panel the radial velocity (y -axis) is plotted against radius (x -axis). Radial velocity perturbations are seen in the density clumps. These perturbations are of order 10 km/s and might be detectable in a real tidal tail with high resolution spectroscopy. Perturbative motions are along the direction of orbital motion in the tidal tail. They are not due to wiggling or bending of the tail. In between the clumps the mean velocities are divergent, and in the clumps they are convergent, consistent with compressive motions due to Jeans instability. There are higher velocity dispersions inside the clumps themselves implying that the development of the instability has heated the tail.

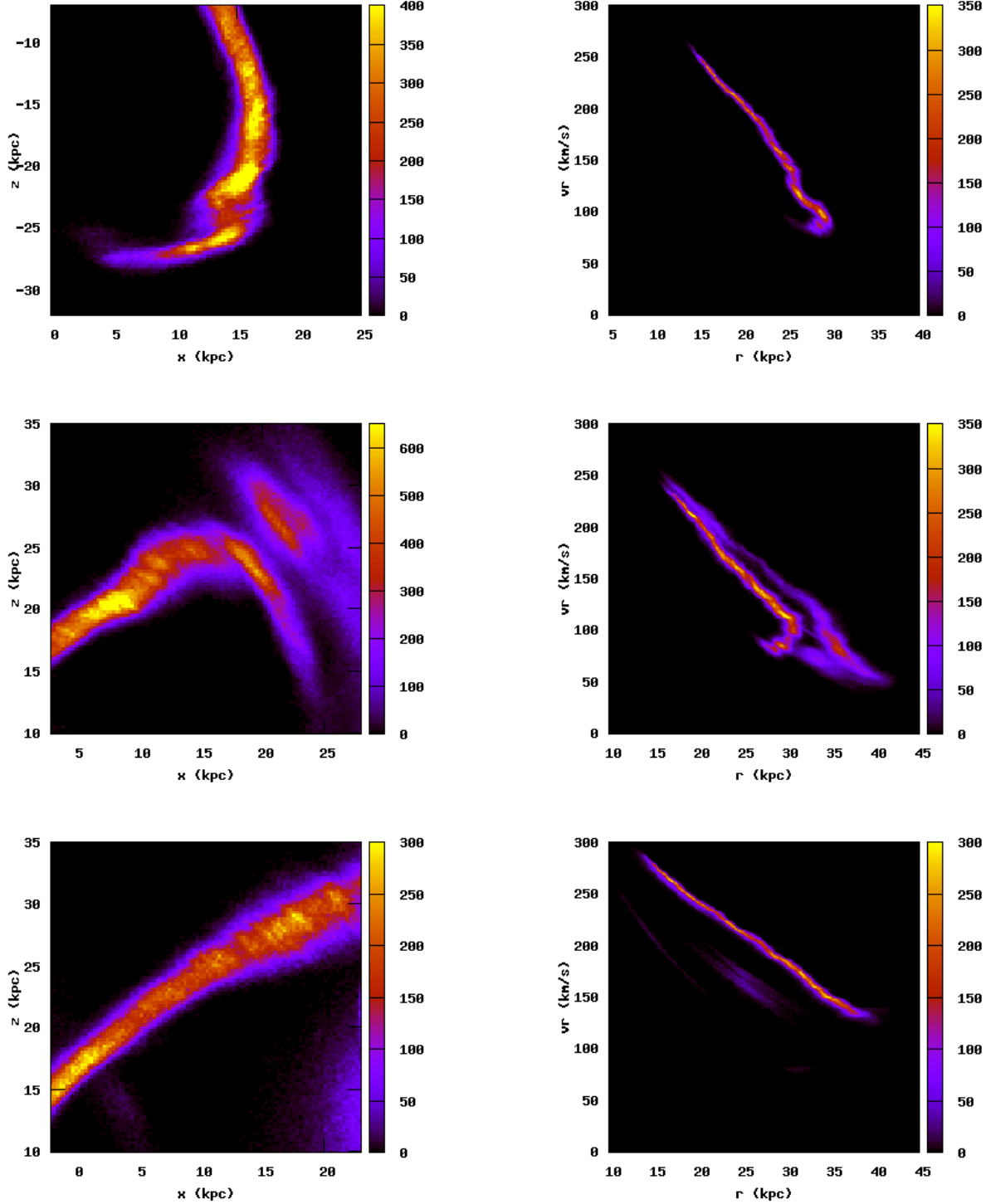


Figure 7. This figure is similar to Figure 6 but for Run 3 and at times (0.77, 1.60, and 1.85 Gyr from top to bottom). Clumps are more closely spaced here than in Run 2. In this simulation the tails are colder and denser because of reduced heating by the halo. As a result the Jeans wavelength is smaller and shorter wavelength perturbations have grown in the tail. Velocity perturbations are smaller than shown in Figure 6 for Run 2 with larger halo particles.